Supporting Online Materials for

Elemental carbon and polycyclic aromatic compounds in a 150-yr sediment core from Lake Qinghai, Tibetan Plateau, China: Influence of regional and local sources and transport paths

Y.M. Han, C. Wei, B.A.M. Bandowe, W. Wilcke, J.J. Cao,
B.Q. Xu, S.P. Gao, X.X. Tie, G.H. Li, Z.D. Jin, Z.S. An

* To whom correspondences should be addressed. E-mail: yongming@ieecas.cn

This file is 26 pages in total, including materials listed below:

S1 Materials and methods;

Figures S1 to S10;

Tables S1 to S2.

S1 Materials and methods

S1.1. Study area and sample collection

Lake Qinghai (36°32′-37°15′ N, 99°36′-100°47′ E), the largest lake in China, has a water surface altitude of 3,194 m above sea level, a surface water area of approximately 4,260 km^2, and a catchment of more than 29,660 km^2 [1]. Under the influence of ASM and westerly climate, the precipitation occurs mainly in summer, contributing most of the annual average values (337 mm a^{-1}), while in winter the area

is covered by ice. The lake is divided into two sub-basins by a NNW-trending piggy-back horst [1], and five major rivers surrounding the lake feed the detrital input into the lake, especially the northern sub-basin (Fig. S1B). The population in the catchment is concentrated in the cities of Gangcha, Tianjun, and Haiyan, which are also located in the northern part. Human activities are therefore expected to have greater influence in the northern part of the lake.

In September 2011, a 33-cm long sediment core QH11-1 was collected from the southern part of Lake Qinghai (in the same place as core QH03-02 from Jin et al. [1]) with a water depth of 28 m using a gravity corer (Uwitec, Austria; Fig. S1B). A distinct water-sediment interface and discernible laminations were observed, indicating a lack of bioturbation and post-depositional disturbance. There was a remarkable litho-stratification between the upper and lower part of the core. Sediments of the upper 6 cm were grey clay, while blackish clay sediments occurred below, which is consistent with previous reports by Xu et al. [2] and Jin et al. [1]. The core was sectioned continuously at 0.5 cm intervals, and then the sediments were freeze-dried, agate mortar ground, and frozen at -20°C until further analysis. The water content and dry density data were estimated from the mass of samples before and after freeze-drying.

Another sediment core QH03-14, located in the northern sub-basin (Fig. S1), and collected in July 2003 and of which the chronology and metal deposition has been reported before [1], was used to compare EC, char, and soot deposition between the southern and northern sub-basins.

S1.2. Chronology reconstruction

The activities of ^{137}Cs, ^{210}Pb, and ^{226}Ra in the depth increments of QH11-1 were analyzed for sediment dating by direct gamma counting of 3-6 g of dried sediments using a multi-channel γ-ray spectrometer (PerkinElmer, GWL-120-15) [1, 3]. The measured ^{210}Pb and ^{137}Cs activities against depth are presented in Fig. S2. Excess ^{210}Pb ($^{210}Pb_{ex}$) activities were calculated from $^{210}Pb_{tot}$ and ^{226}Ra activities with the level-by-level method. The activity of excess $^{210}Pb_{ex}$ in the uppermost 1-cm section of core QH11-1 in our study (about 478.25 Bq kg^{-1}) is similar to that reported by Jin et al [1] (474.3 Bq kg^{-1}), who collected the sediment core from the same site as we did. However, our activitives are higher than those reported by others in the southern basin [4, 5], which may be associated with sediment focusing [6] as our cores (collected in 2003 and in 2011, respectively) were obtained in deeper water than most previous cores. However, the $^{210}Pb_{ex}$ activity in the surface sediment of core QH11-1 is much lower than that in the northern sub-basin [1, 2] because of more detrital inputs in the north sub-basin of the lake. ^{137}Cs exhibited a peak, which is similar with other cores collected in the Lake Qinghai[1, 2, 5] and this suggests that substantial mixing of the sediments did not occur. Similarly, higher ^{137}Cs concentrations were found in the cores of northern sub-basin[1, 2, 5].

Fig. S2 presents the chronology reconstruction for core QH11-1 using the constant rate of ^{210}Pb supply (CRS) model[7-9] and the corresponding accumulation rates. The unconstrained CRS model predicts the ^{137}Cs peak (58.1 Bq kg^{-1}) at 3.25 cm sediment depth to AD 1977 ± 3.4, which is not in agreement with the global nuclear

bomb testing period of ~1963. However, the 3.75 cm sediment depth corresponds to AD 1966 ± 4.4, which is very close to the global nuclear fallout (Fig. S2C). Calculating the ^{137}Cs fluxes using mass accumulation rates (MARs) as derived from the CRS model[7, 8] (Fig. S2F) demonstrates that the shape of the ^{137}Cs peak is really broad and it is difficult to define when the maximum flux occurred. This points to post-deposition diffusional redistribution of ^{137}Cs in the sediment profile which is also supported by the ^{137}Cs activity data that appeared to be moved downward the core (Figs S2E). The constrained CRS model[9] that forces the chronology through the ^{137}Cs fix-point (3.75 cm = AD 1963) yields a chronology (Fig. S2D) very close to that reconstructed using the CRS model. Thus, the "free-shape CRS model"[7-9] was used in our study for chronology reconstruction.

S1.3. EC, char, and soot measurement

The IMPROVE (Interagency Monitoring of Protected Visual Environments) method was used to quantify EC, char, and soot concentrations following Han et al. [10, 11]. Briefly, ~100 mg sediment for each sample was pretreated with hydrochloric and hydrofluoric acids to remove carbonate, metal oxides, and silicates. The pretreated residues were then filtered through pre-baked (850°C for 3 hours) quartz-fiber filters (0.4 μm pore size, Whatman) using deionized water and air dried in an oven (35°C for 8 hours). A DRI Thermal/Optical Carbon Analyzer (Atmoslytic Inc. Calabasas, CA) was used to implement the IMPROVE protocol. It reports four OC fractions (OC1 to OC4 at 120, 250, 450 and 550°C in a pure helium atmosphere), three EC fractions (EC1 to EC3 at 550, 700 and 800°C in 2% oxygen/98% helium atmosphere), and one

pyrolyzed organic carbon (POC) fraction. The POC produced in the inert atmosphere is monitored by a laser to both the reflectance and transmittance during thermal analysis. The IMPROVE protocol defined EC as the sum of the three EC fractions minus POC. Han et al. [12] defined char as EC1 minus POC, while soot as the sum of EC2 and EC3.

We are aware of the fact that the methodology for BC measurement is disputed [13]. The comparison of the different methods traditionally used for geological samples showed that the BC concentrations determined with different methods can vary by a factor of up to 571 [14]. For aerosols, the most commonly used method is the thermal optical method with different protocols, and the concentrations measured by the different protocols for given samples on average, only varies by a factor of 2 [15], which is much narrower than the wide range of measured concentrations caused by the different methods used for geological samples. To ensure quality control and validation of the analytical method, standard reference materials (SRMs) need to be included into analytical protocols, which is mostly not the case. Furthermore, possible matrix effects have to be accounted for.

For several decades, the thermal optical method was mainly used to quantify aerosol EC concentrations [16]. Just since 2007, it was extended to measure EC in sediments and soils [10, 17]. Based on the finding that char and soot in standard reference materials (SRMs) can be stepwise oxidized in the EC1 and EC2+3 steps, respectively, it was proposed that the IMPROVE method can be used to differentiate between char and soot [12]. The adaptation, validation and application of this method have been tested

in many previous studies. Positive and negative EC SRMs and environmental EC matrices [13] were tested in many previous studies [10, 11, 18]. In addition, Han et al. [19] demonstrated that the soot concentrations determined with the IMPROVE method (i.e. the sum of the EC2+3 steps) compared well with soot concentrations determined with the chemothermal (CTO-375) method designed to specifically measure soot carbon [20-22].

In the meantime, the application of the IMPROVE method to differentiate between char and soot has been extended to aerosols [23-28], sediments and soils [19, 29, 30]. All these studies have shown that the IMPROVE protocol delivers results which reasonably reflect the char and soot contributions to EC in the samples. For example, the char/soot ratio was successfully used to distinguish different sources in aerosol studies [28, 31]. A study of the spatial distribution of char and soot in urban, rural, and remote areas [27] revealed that char has local sources and is not far transported, while soot is regionally dispersed, which is in line with our knowledge about the larger particle size of char than of soot [32]. The 150 yr historic reconstruction of char and soot deposition from several sediment cores in eastern China [19] showed similar historical profiles for soot but different ones for char, which further confirms the different transport modes of char and soot. The sedimentary soot profiles [19] well reflect the industrialization history of China, showing an abrupt increase in the late 1970s, the timing of opening and economic reform of China. The stronger association of PAHs with soot than with char in soils and sediments in the Guanzhong Basin in China [33] is consistent with the results of the previous SRM test that showed a higher absorption

capacity of PAHs by soot than by char [34]. The Holocene char and soot records reconstructed from Lake Daihai reflected the paleo-wildfire occurrence and they showed good correlations with climate changes and human activities [29].

In recent years, brown carbon (BrC) has received increasing attention as a type of carbonaceous aerosol which also absorbs light [35]. The light-absorbing characteristics of BrC [35] and char [24] both are specific for certain wavelengths of the light spectrum, and their light absorption is weaker than that of soot. BrC and char are distinctively different. Char (or charcoal) particles are combustion residues that are inert and can exist in the environment millions of years [36], whereas BrC is water soluble and considerably more labile. Quantification methods of BrC and char are different. Char is operationally measured as the carbon that remains after chemical or thermal pretreatment [12, 37-39], whereas BrC is measured as the carbon extractable by water or organic solvents [35, 40, 41].

S1.4. PAHs, OPAHs and AZAs analyses

Concentration of 29 parent- and alkyl-PAHs, 15 OPAHs and 4 azaarenes (AZAs) were determined. A mixture of 7 deuterated PAHs and 2 deuterated OPAHs were used as internal standard to quantify parent-/alkyl-PAHs and carbonyl-OPAHs, respectively. A detailed description of the analytical procedure for the measurement is given by Bandowe and Wilcke [42, 43]. Briefly, about 2 g of sediment sample, 25 μL of each of the deuterated OPAHs and PAHs mixtures were added as internal standards to the accelerated solvent extractor (ASE) cell. Samples were extracted using ASE 200 (Dionex, Sunnyvale, CA, USA) with dichloromethane in a first extraction cycle, and

157 with $CH_3COCH_3/CH_2C_{l2}/CF_3COOH$ (1%) (250:125:1 v/v/v) in a second extraction
158 cycle. The two extracts of each sample were combined, dried on Na_2SO_4, and cleaned
159 up/fractionated on silica gel (10% deactivated) columns. The PAHs fraction was
160 eluted with 15 mL hexane/dichloromethane (5:1 v/v), followed by 8 mL
161 dichloromethane and 5 mL acetone to elute OPAHs and AZAs. The PAHs and OPAHs
162 + AZAs fractions were rotary evaporated to about 0.5 mL, transferred to a 2 mL GC
163 vial, spiked with 25 μL (22 μg/mL) fluoranthene-D_{10} as recovery standard, put in the
164 refrigerator and followed by GC/MS measurement.

165 An Agilent 7890A gas chromatograph coupled to an Agilent 5975C mass
166 spectrometer in EI and SIM mode was used for measurements. The GC Oven program
167 for PAHs, OPAHs, and AZAs was the same as in previous papers [43, 44]. All data
168 recording and processing was done with the Agilent MSD ChemStation software
169 package.

170 Target compounds were quantified by the internal standard technique using
171 seven calibration standards prepared from target compound standards each spiked
172 with a constant concentration of internal standard. IBM SPSS 19.0 for Windows and
173 Origin 8.5 were used for statistical analysis and graphics.

174 **S1.5. Quality assurance and quality control**

175 All glassware was rinsed with acetone, machine-washed, baked at 250 °C for
176 12 h, and rinsed with high purity solvents before use. All solvents used for extraction,
177 column chromatography, and standard preparation were high purity for pesticide
178 residue analysis. To check and correct for possible contaminations during the

179 analytical procedure, we processed blanks made of diatomaceous earth at the
180 beginning of each batch of 24 samples. Most compounds were either not detected in
181 the blanks or were measured in negligible quantities, significantly below those found
182 in the samples. The measured compound concentrations in the samples were corrected
183 by subtracting the mean blank concentrations. We checked the accuracy of PAH
184 measurements by including the certified reference material ERM-CC013a (BAM,
185 Berlin, Germany) into our analyses. The mean recovery of all PAHs for which
186 certified values were provided was 110%. We checked the recovery of all internal
187 standards. The mean recovery of deuterated PAHs and OPAHs was 80% (67-88%).
188 All concentrations are reported without recovery correction.
189

References

1. Jin, Z.; Han, Y.; Chen, L., Past atmospheric Pb deposition in Lake Qinghai, northeastern Tibetan Plateau. *J. Paleolimnol.* **2010,** 43, (3), 551-563.

2. Xu, H.; Ai, L.; Tan, L.; An, Z., Geochronology of a surface core in the northern basin of Lake Qinghai: evidence from 210 Pb and 137 Cs radionuclides. *Chinese J. Geochem.* **2006,** 25, 301-306.

3. Han, Y. M.; Cao, J. J.; Kenna, T. C.; Yan, B. Z.; Jin, Z. D.; Wu, F.; An, Z. S., Distribution and ecotoxicological significance of trace element contamination in a similar to 150 yr record of sediments in Lake Chaohu, Eastern China. *J. Environ. Monitor.* **2011,** 13, (3), 743-752.

4. Henderson, A. C. G.; Holmes, J. A.; Zhang, J.; Leng, M. J.; Carvalho, L. R., A carbon-and oxygen-isotope record of recent environmental change from Qinghai Lake, NE Tibetan Plateau. *Chinese Science Bulletin* **2003,** 48, (14), 1463-1468.

5. Shen, J.; Zhang, E.; Xia, W., Records from lake sediments of Lake Qinghai to mirror climatic and environmental changes of the past about 1000 years. *Quaternary Sciences* **2001,** 21, 508-513.

6. Hilton, J.; Lishman, J. P.; Allen, P. V., The Dominant Processes of Sediment Distribution and Focusing in a Small, Eutrophic, Monomictic Lake. *Limnology and Oceanography* **1986,** 31, (1), 125-133.

7. Appleby, P., Chronostratigraphic techniques in recent sediments. In *Tracking environmental change using lake sediments*, Last, W. M.; Smol, J. P., Eds. Springer: 2001; pp 171-203.

8. Appleby, P. G., Three decades of dating recent sediments by fallout radionuclides: a review. *Holocene* **2008,** 18, (1), 83-93.

9. von Gunten, L.; Grosjean, M.; Beer, J.; Grob, P.; Morales, A.; Urrutia, R., Age modeling of young non-varved lake sediments: methods and limits. Examples from two lakes in Central Chile. *J. Paleolimnol.* **2009,** 42, (3), 401-412.

10. Han, Y. N.; Cao, J. J.; An, Z. S.; Chow, J. C.; Watson, J. G.; Jin, Z.; Fung, K.; Liu, S. X., Evaluation of the thermal/optical reflectance method for quantification of elemental carbon in sediments. *Chemosphere* **2007,** 69, 526-533.

11. Han, Y. M.; Cao, J. J.; Posmentier, E. S.; Chow, J. C.; Watson, J. G.; Fung, K. K.; Jin, Z. D.; Liu, S. X.; An, Z. S., The effect of acidification on the determination of elemental carbon, char-, and soot-elemental carbon in soils and sediments. *Chemosphere* **2009,** 75, (1), 92-99.

12. Han, Y. M.; Cao, J. J.; Chow, J. C.; Watson, J. G.; An, Z. S.; Jin, Z. D.; Fung, K. C.; Liu, S. X., Evaluation of the thermal/optical reflectance method for discrimination between char- and soot-EC. *Chemosphere* **2007,** 69, 569-574.

13. Hammes, K.; Schmidt, M. W. I.; Smernik, R. J.; Currie, L. A.; Ball, W. P.; Nguyen, T. H.; Louchouarn, P.; Houel, S.; Gustafsson, O.; Elmquist, M.; Cornelissen, G.; Skjemstad, J. O.; Masiello, C. A.; Song, J.; Peng, P. a.; Mitra, S.; Dunn, J. C.; Hatcher, P. G.; Hockaday, W. C.; Smith, D. M.; Hartkopf-Froeder, C.; Boehmer, A.; Lueer, B.; Huebert, B. J.; Amelung, W.; Brodowski, S.; Huang, L.; Zhang, W.; Gschwend, P. M.; Flores-Cervantes, D. X.; largeau, C.; Rouzaud, J.-N.; Rumpel, C.; Guggenberger, G.; Kaiser, K.; Rodionov, A.; Gonzalez-Vila, F. J.; Gonzalez-Perez, J. A.; de la Rosa, J. M.; Manning, D. A. C.; Lopez-Capel, E.; Ding, L., Comparison of quantification methods to measure fire-derived (black/elemental) carbon in soils and sediments using reference materials from soil, water, sediment and the atmosphere. *Global Biogeochem. Cycles* **2007,** 21, (3), DOI: 10.1029/2006GB002914.

14. Schmidt, M. W. I.; Skjemstad, J. O.; Czimczik, C. I.; Glaser, B.; Prentice, K. M.; Gelinas, Y.; Kuhlbusch, T. A. J., Comparative analysis of black carbon in soils. *Global Biogeochem. Cycles* **2001,**

15, (1), 163-167.
15. Watson, J. G.; Chow, J. C.; Chen, L.-W. A., Summary of organic and elemental carbon/black carbon analysis methods and intercomparisons. *J. Aero. Air Qual. Res.* **2005,** 5, 65-102.
16. Chow, J. C.; Watson, J. G.; Pritchett, L. C.; Pierson, W. R.; Frazier, C. A.; Purcell, R. G., The dri thermal/optical reflectance carbon analysis system: description, evaluation and applications in U.S. Air quality studies. *Atmospheric Environment. Part A. General Topics* **1993,** 27, (8), 1185-1201.
17. Husain, L.; Khan, A. J.; Ahmed, T.; Swami, K.; Bari, A.; Webber, J. S.; Li, J., Trends in atmospheric elemental carbon concentrations from 1835 to 2005. *J. Geophys. Res.* **2008,** 113, (D13), doi:10.1029/2007JD009398.
18. Han, Y.; Chen, A.; Cao, J.; Fung, K.; Ho, F.; Yan, B.; Zhan, C.; Liu, S.; Wei, C.; An, Z., Thermal/Optical Methods for Elemental Carbon Quantification in Soils and Urban Dusts: Equivalence of Different Analysis Protocols. *Plos One* **2013,** 8, (12), Doi:10.1371/journal.pone.0083462.
19. Han, Y. M.; Cao, J. J.; Yan, B. Z.; Kenna, T. C.; Jin, Z. D.; Cheng, Y.; An, Z. S., Comparison of elemental carbon in lake sediments measured by TOR, TOT and CTO methods and 150-year pollution history in Eastern China. *Environ. Sci. Technol.* **2011,** 45, (12), 5287-5293.
20. Gustafsson, O.; Gschwend, P. M., Soot as a strong partition medium for polycyclic aromatic hydrocarbons in aquatic systems. In *Molecular Markers in Environmental Geochemistry*, 1997; Vol. 671, pp 365-381.
21. Elmquist, M.; Cornelissen, G.; Kukulska, Z.; Gustafsson, O., Distinct oxidative stabilities of char versus soot black carbon: Implications for quantification and environmental recalcitrance. *Global Biogeochem. Cycles* **2006,** 20, GB2009, doi:10.1029/2005GB002629.
22. Nguyen, T. H.; Brown, R. A.; Ball, W. P., An evaluation of thermal resistance as a measure of black carbon content in diesel soot, wood char, and sediment. *Org. Geochem.* **2004,** 35, (3), 217-234.
23. Han, Y. M.; Han, Z. W.; Cao, J. J.; Chow, J. C.; Watson, J. G.; An, Z. S.; Liu, S. X.; Zhang, R. J., Distribution and origin of carbonaceous aerosol over a rural high-mountain lake area, Northern China and its transport significance. *Atmos. Environ.* **2008,** 42, (10), 2405-2414.
24. Han, Y. M.; Cao, J. J.; Lee, S. C.; Ho, K. F.; An, Z. S., Different characteristics of char and soot in the atmosphere and their ratio as an indicator for source identification in Xi'an, China. *Atmos. Chem. Phys.* **2010,** 10, (2), 595-607.
25. Kim, K. H.; Sekiguchi, K.; Furuuchi, M.; Sakamoto, K., Seasonal variation of carbonaceous and ionic components in ultrafine and fine particles in an urban area of Japan. *Atmos. Environ.* **2011,** 45, (8), 1581-1590.
26. Lim, S.; Lee, M.; Lee, G.; Kim, S.; Yoon, S.; Kang, K., Ionic and carbonaceous compositions of PM10, PM2.5 and PM1.0 at Gosan ABC Superstation and their ratios as source signature. *Atmos. Chem. Phys.* **2012,** 12, (4), 2007-2024.
27. Jeong, C.-H.; Herod, D.; Dabek-Zlotorzynska, E.; Ding, L.; McGuire, M. L.; Evans, G., Identification of the Sources and Geographic Origins of Black Carbon using Factor Analysis at Paired Rural and Urban sites. *Environ. Sci. Technol.* **2013,** 47, (15), 8462-8470.
28. Minoura, H.; Morikawa, T.; Mizohata, A.; Sakamoto, K., Carbonaceous aerosol and its characteristics observed in Tokyo and south Kanto region. *Atmos. Environ.* **2012,** 61, 605-613.
29. Han, Y. M.; Marlon, J.; Cao, J. J.; Jin, Z. D.; An, Z. S., Holocene linkages between char, soot, biomass burning and climate from Lake Daihai, China. *Global Biogeochem. Cycles* **2012,** 26, doi:10.1029/2012GB004413.
30. Cong, Z.; Kang, S.; Gao, S.; Zhang, Y.; Li, Q.; Kawamura, K., Historical Trends of Atmospheric

278 Black Carbon on Tibetan Plateau As Reconstructed from a 150-Year Lake Sediment Record. *Environ.*
279 *Sci. Technol.* **2013,** 47, (6), 2579-2586.
280 31. Han, Y. M.; Lee, S. C.; Cao, J. J.; Ho, K. F.; An, Z. S., Spatial distribution and seasonal variation
281 of char-EC and soot-EC in the atmosphere over China. *Atmos. Environ.* **2009,** 43, (38), 6066-6073.
282 32. Masiello, C. A., New directions in black carbon organic geochemistry. *Mar. Chem.* **2004,** 92, (1-4),
283 201-213.
284 33. Han, Y. M.; Bandowe, B. A. M.; Wei, C.; Cao, J. J.; Wilcke, W.; Wang, G. H.; Ni, H. Y.; Jin, Z. D.;
285 An, Z. S.; Yan, B. Z., Stronger association of polycyclic aromatic hydrocarbons with soot than with
286 char in soils and sediments. *Chemosphere* **2015,** 119, 1335-1345.
287 34. Cornelissen, G.; Gustafsson, O.; Bucheli, T. D.; Jonker, M. T. O.; Koelmans, A. A.; Van Noort, P.
288 C. M., Extensive sorption of organic compounds to black carbon, coal, and kerogen in sediments and
289 soils: Mechanisms and consequences for distribution, bioaccumulation, and biodegradation. *Environ.*
290 *Sci. Technol.* **2005,** 39, (18), 6881-6895.
291 35. Andreae, M. O.; Gelencser, A., Black carbon or brown carbon? The nature of light-absorbing
292 carbonaceous aerosols. *Atmos. Chem. Phys.* **2006,** 6, 3131-3148.
293 36. Scott, A. C.; Glasspool, I. J., The diversification of Paleozoic fire systems and fluctuations in
294 atmospheric oxygen concentration. *Proc. Natl. Acad. Sci.* **2006,** 103, (29), 10861-10865.
295 37. Lim, B.; Cachier, H., Determination of black carbon by chemical oxidation and thermal treatment
296 in recent marine and lake sediments and Cretaceous-Tertiary clays. *Chem. Geol.* **1996,** 131, (1-4),
297 143-154.
298 38. Masiello, C. A.; Druffel, E. R. M., Black carbon in deep-sea sediments. *Science* **1998,** 280, (5371),
299 1911-1913.
300 39. Bird, M. I.; Grocke, D. R., Determination of the abundance and carbon isotope composition of
301 elemental carbon in sediments. *Geochim. Cosmochim. Acta* **1997,** 61, (16), 3413-3423.
302 40. Lukacs, H.; Gelencser, A.; Hammer, S.; Puxbaum, H.; Pio, C.; Legrand, M.; Kasper-Giebl, A.;
303 Handler, M.; Limbeck, A.; Simpson, D.; Preunkert, S., Seasonal trends and possible sources of brown
304 carbon based on 2-year aerosol measurements at six sites in Europe. *J. Geophys. Res.* **2007,** 112, (D23),
305 DOI: 10.1029/2006JD008151.
306 41. Graber, E. R.; Rudich, Y., Atmospheric HULIS: How humic-like are they? A comprehensive and
307 critical review. *Atmos. Chem. Phys.* **2006,** 6, 729-753.
308 42. Bandowe, B. A. M.; Wilcke, W., Analysis of Polycyclic Aromatic Hydrocarbons and Their
309 Oxygen-Containing Derivatives and Metabolites in Soils. *Journal of Environmental Quality* **2010,** 39,
310 (4), 1349-1358.
311 43. Bandowe, B. A. M.; Sobocka, J.; Wilcke, W., Oxygen-containing polycyclic aromatic
312 hydrocarbons (OPAHs) in urban soils of Bratislava, Slovakia: Patterns, relation to PAHs and vertical
313 distribution. *Environ. Pollut.* **2011,** 159, (2), 539-549.
314 44. Bandowe, B. A. M.; Shukurov, N.; Kersten, M.; Wilcke, W., Polycyclic aromatic hydrocarbons
315 (PAHs) and their oxygen-containing derivatives (OPAHs) in soils from the Angren industrial area,
316 Uzbekistan. *Environ. Pollut.* **2010,** 158, (9), 2888-2899.
317

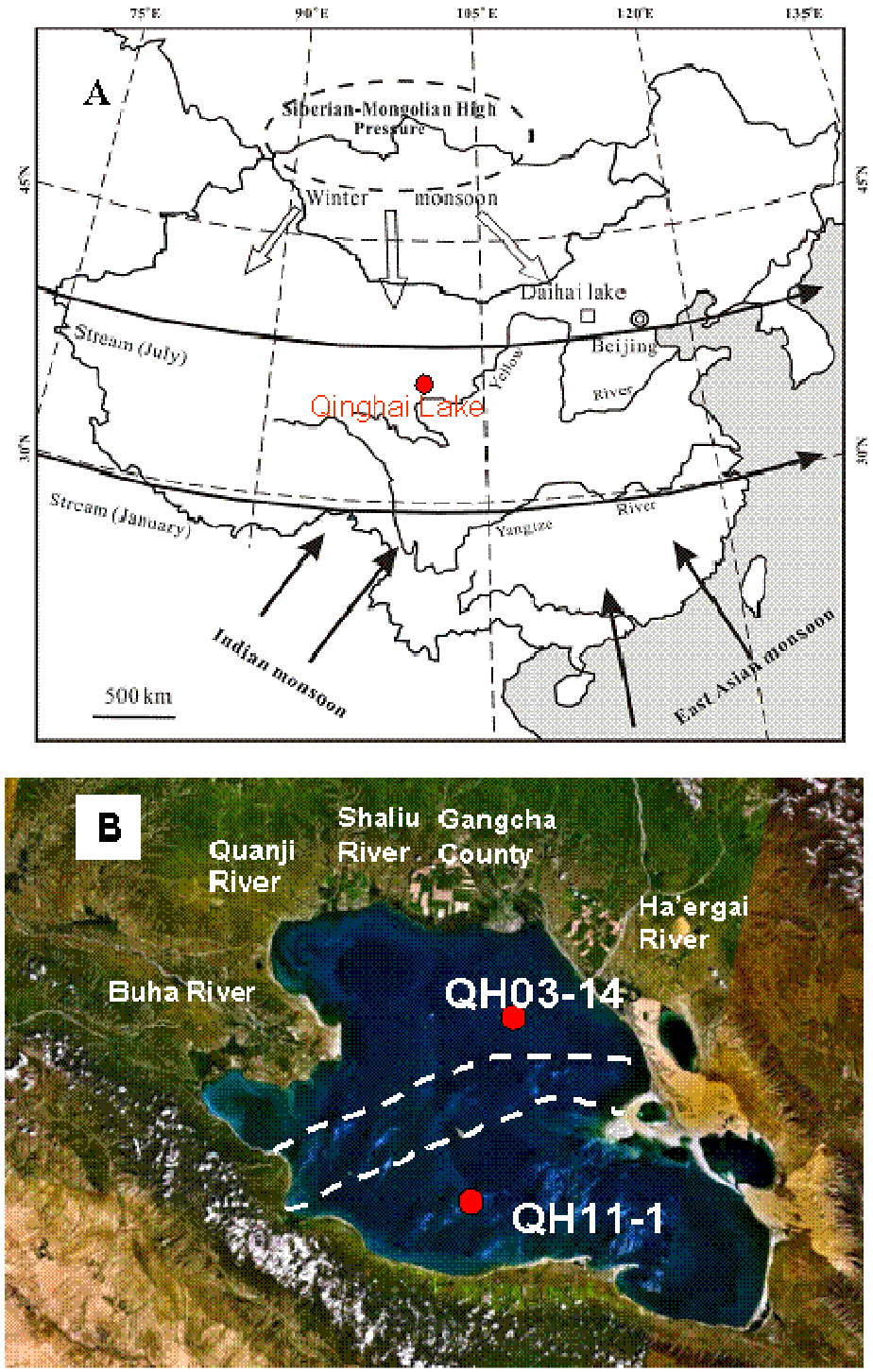

Fig. S1. (A) Climatic systems of China, including the East Asian and Indian summer monsoons, the Siberian–Mongolian High, and the Westerlies. (B) Location of the sediment cores QH03-14 and QH11-1 obtained from different sub-basins of Lake Qinghai.

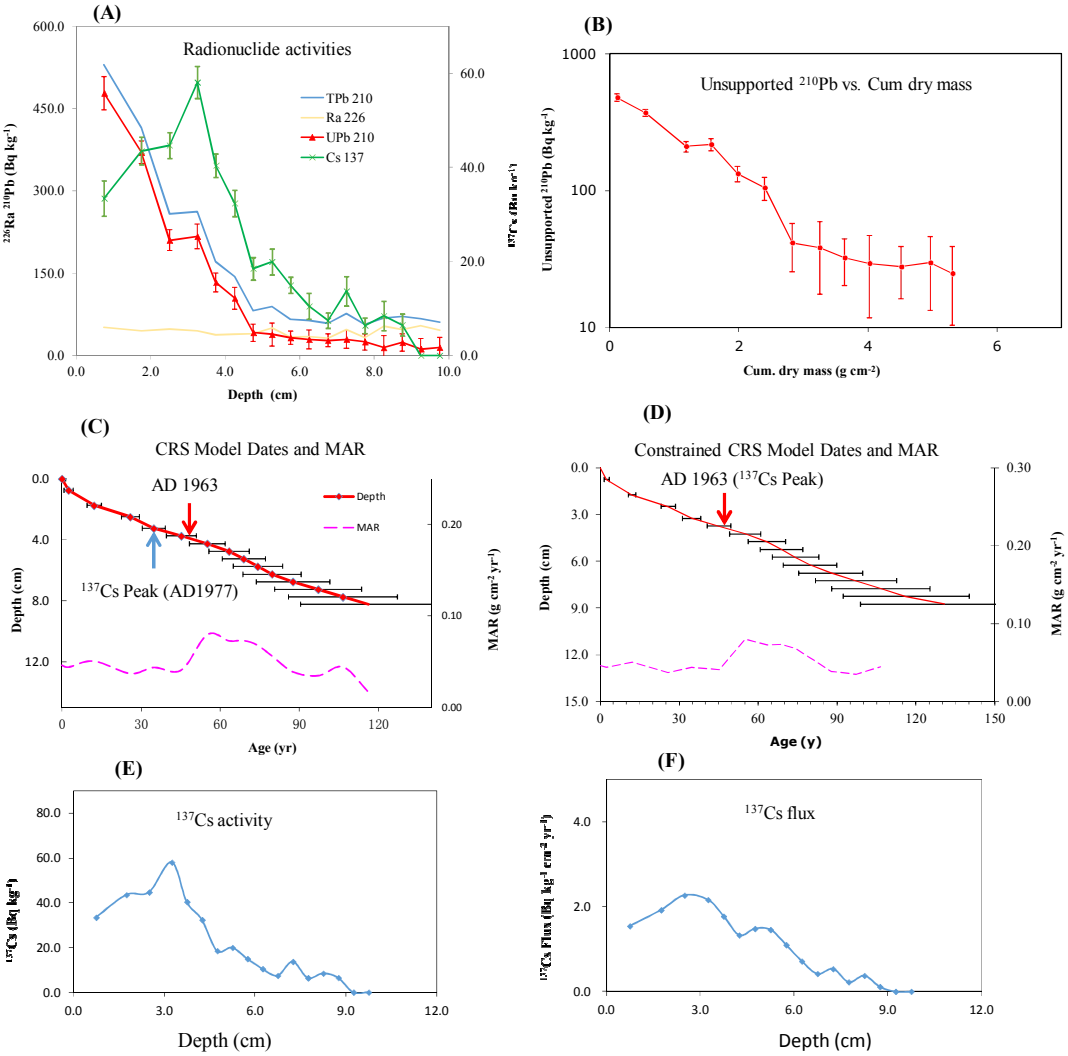

Fig. S2. Chronology reconstruction of core QH11-1 using the constant rate of supply (CRS) ^{210}Pb model. (A) Measured Pb, Cs, and Ra activities, including total ^{210}Pb (blue line), excess ^{210}Pb (red line with error bars), ^{226}Ra (cyan line), and ^{137}Cs (green line with error bars) concentrations along with depth variation; (B) Excess ^{210}Pb against cumulative mass; (C) CSR model dates and corresponding mass accumulation rate (MAR), which show that ^{137}Cs peak at 3.25 sediment depth occurs at ~1977; (D) Constrained (3.75 cm through 1963) CRS model dates and corresponding MAR; (E) ^{137}Cs peak vs. depth presenting one ^{137}Cs peak; (F) ^{137}Cs flux calculated using the CRS model vs. depth presenting that the shape of the ^{137}Cs peak is broad.

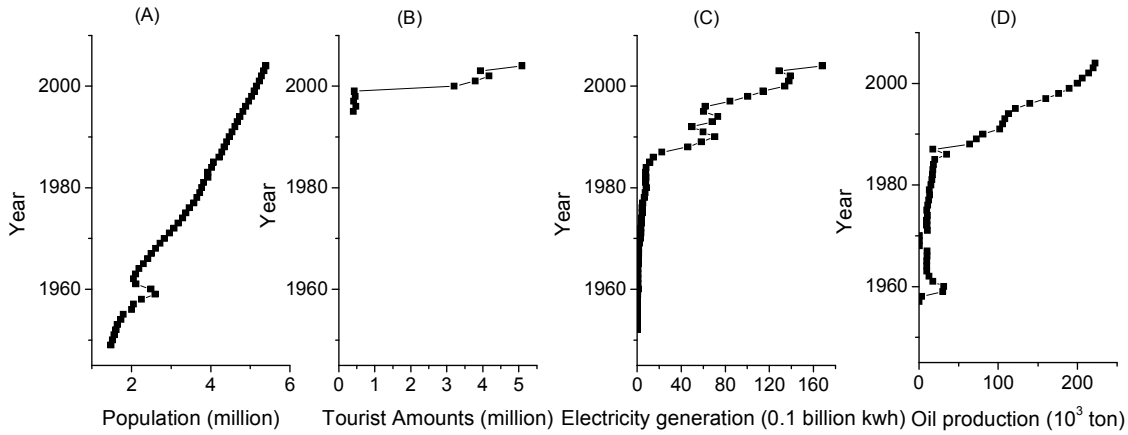

Fig. S3. History of the population numbers, number of tourists, extents of electricity generation and oil production (or consumption) in Qinghai Province in the past 60 years. Tourism in Qinghai Province is mainly driven by in the attractions around Lake Qinghai.

345
346

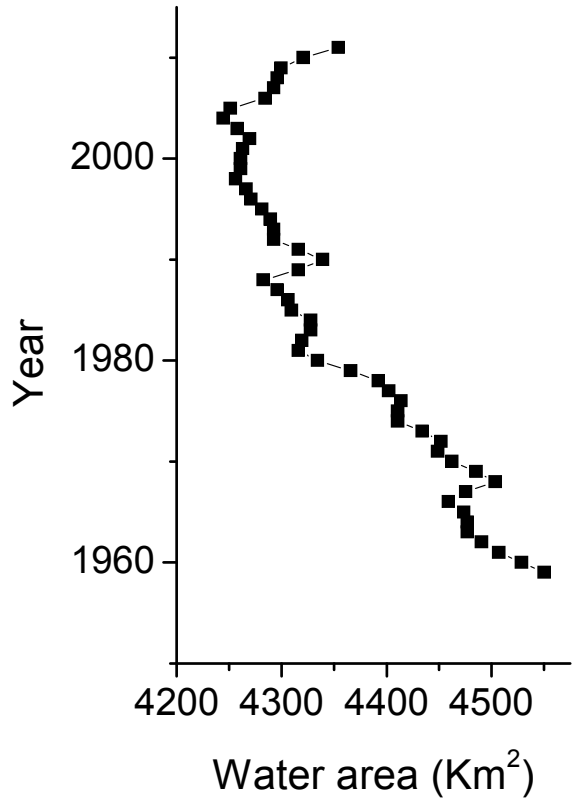

347

348 **Fig. S4.** History of the surface size of Lake Qinghai in the past 50 years.

349

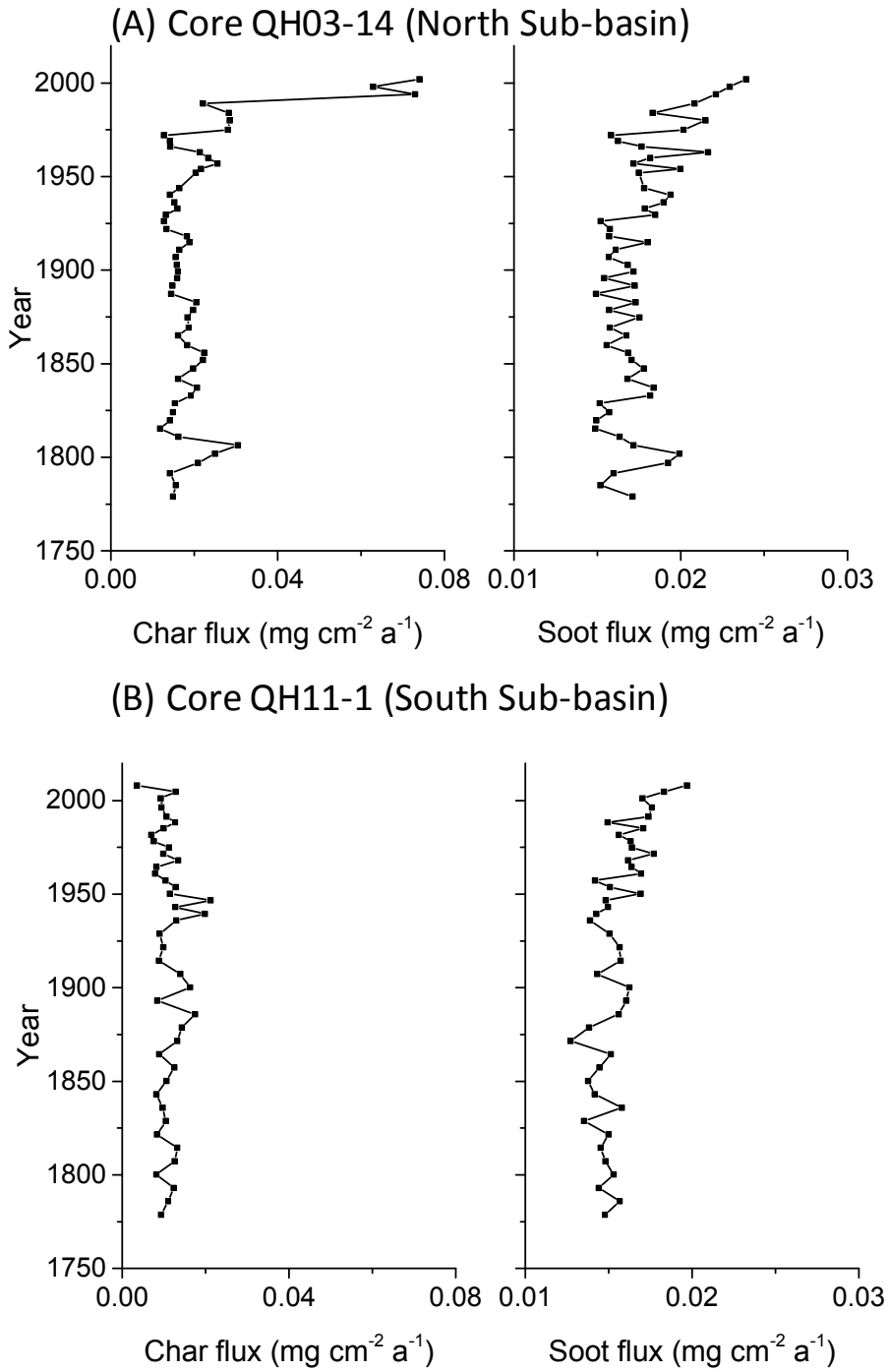

Fig. S5. Historical profiles of char and soot fluxes in (A) sediment core QH03-14 (northern sub-basin with more human inputs) and (B) sediment core QH11-1 (southern sub-basin).

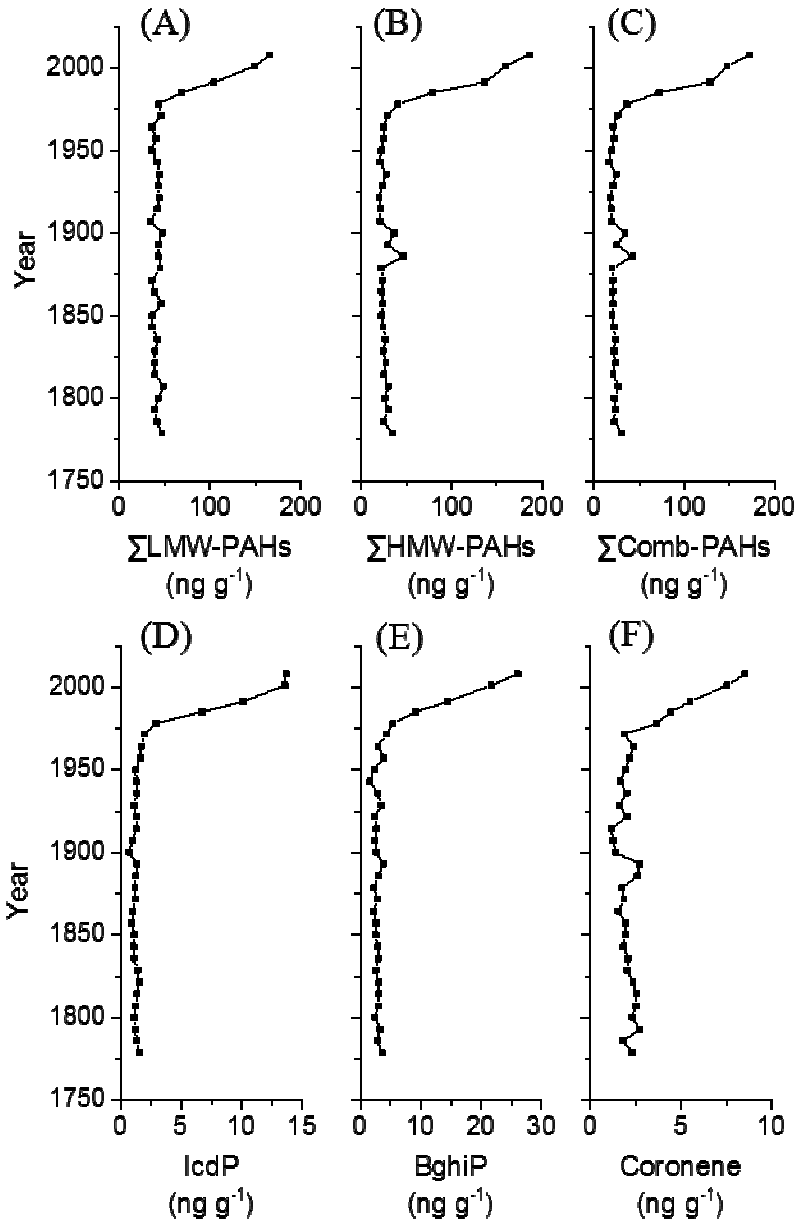

Fig. S6. Vertical distribution of the concentrations (ng g^{-1}) of (A) ∑LMW-PAHs; (B) ∑HMW-PAHs; (C) ∑COMB-PAHs; (D) IcdP (indeno[c,d]pyrene); (E) BghiP (benzo[g,h,i]perylene; and (F) Coronene. See main text and Table S1 for the definition of abbreviations.

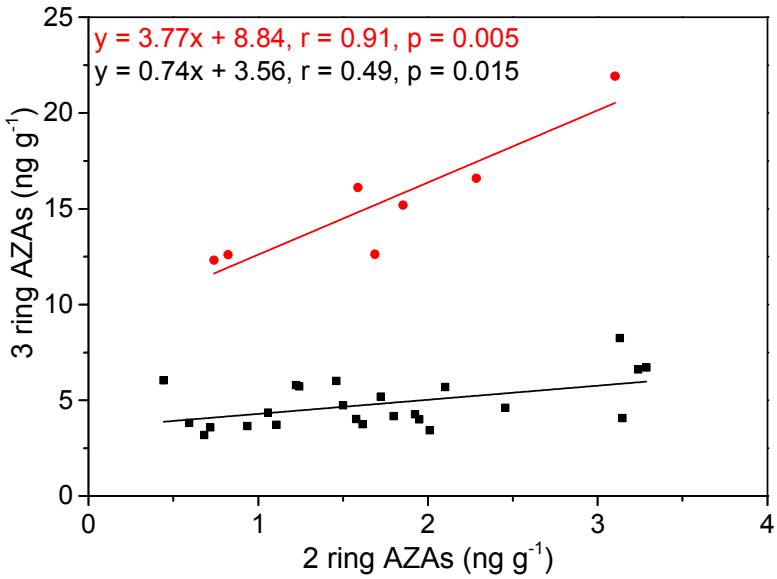

Fig. S7. Relationship between the concentrations of 2-ring and 3-ring azaarenes (AZAs) in sediments of Lake Qinghai before (dark squares) and after (red cycles) the 1960s. The considered 2-ring azaarene is quinoline, while 3-ring azaarenes include benzo[h]quinoline, acridine and carbazole.

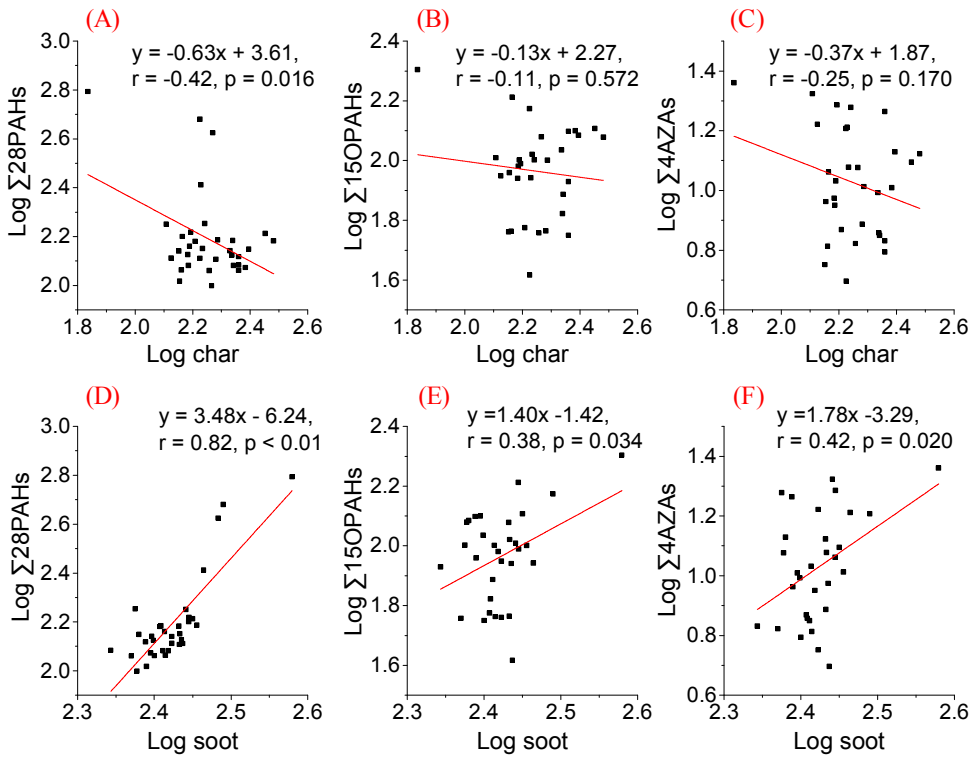

Fig. S8. Relationships between the concentrations of (A) ∑28PAHs (total measured PAHs without perylene) vs char, (B) ∑15OPAHs vs char, (C) ∑4AZAs vs char, (D) ∑28PAHs vs soot, (E) ∑15OPAHs vs soot, and (F) ∑4AZAs vs soot. Concentrations of PAHs, OPAHs, AZAs (ng g^{-1}) and char, soot (mg g^{-1}) are log-transferred.

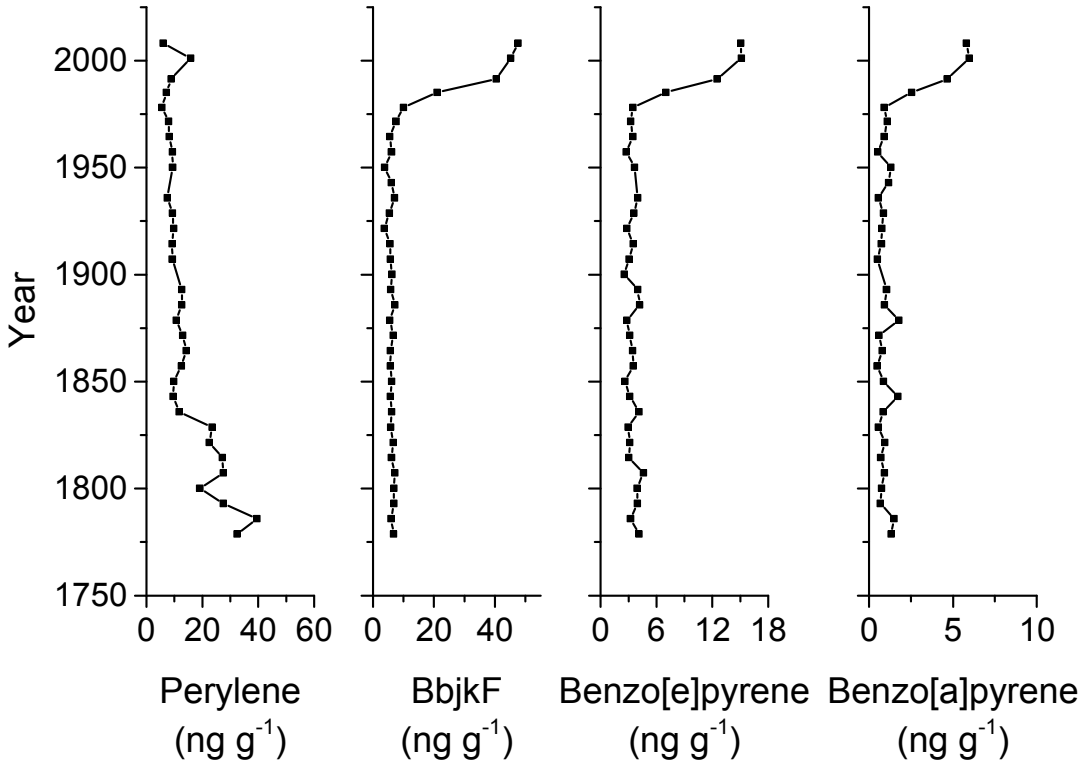

Fig S9. Vertical distribution of the concentrations of (A) perylene and its combustion-derived isomers (MW = 252) such as (B) benzo[b+j+k]fluoranthene (BbjkF), (C) benzo[e]pyrene and (D) benzo[a]pyrene in the sediment core QH11-1 of Lake Qinghai. benzo[b+j+k]fluoranthene is sum of benzo[b]fluoranthene, benzo[j]fluoranthene and benzo[k]fluoranthene.

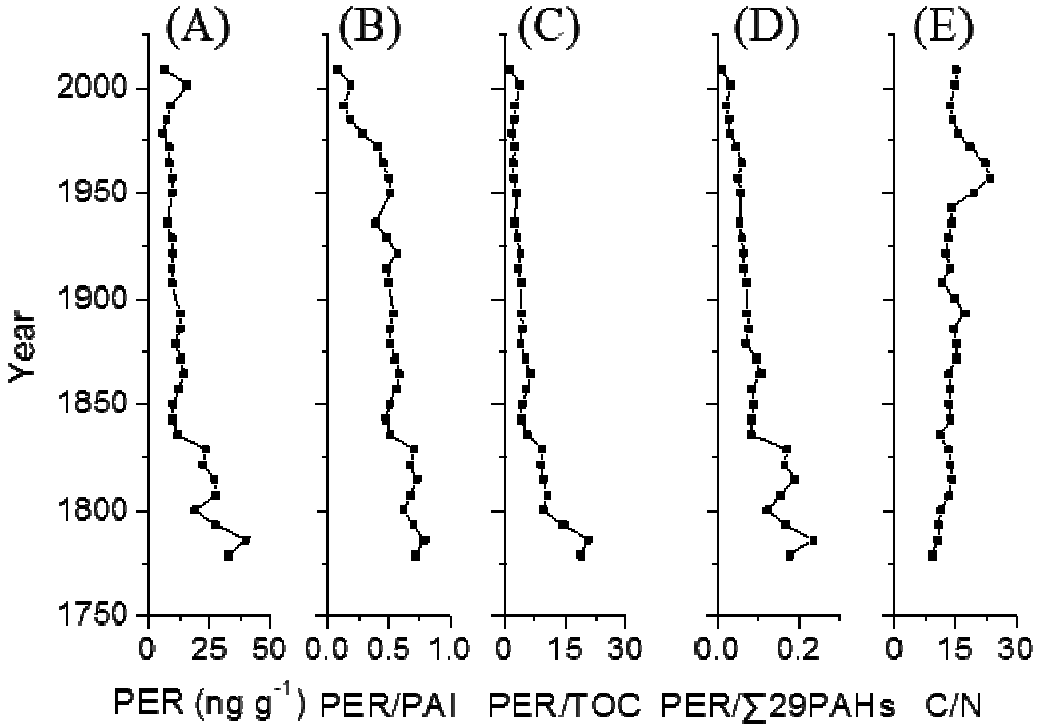

Fig. S10. (A) Perylene (PER) concentrations, and concentration ratios of (B) PER to its penta-aromatic isomers (PER/PAI), (C) concentration ratio of PER/total organic carbon (TOC), (D) concentration ratio of PER/sum of 29 PAHs (∑29PAHs, including perylene), and of (E) TOC to total nitrogen concentrations (C/N) in Lake Qinghai.

404

405 **Table S1.** Statistical description concentrations of PACs, sum of concentrations of
406 PACs and other sediment properties.

	Abbreviation	Minimum	Maximum	Average	Max/Min
azaarenes	AZAs				
Quinoline	QUI	0.44	3.29	1.71	7.4
Benzo[h]quinoline	BhQ	0.48	13.2	3.51	27.7
Acridine	ACR	0.57	5.73	1.11	10.1
Carbazole	CAR	1.81	3.84	2.57	2.1
Oxygenated PAHs	OPAHs				
1-Indanone	1-IND	1.02	10.2	4.55	9.9
1,4-Naphthoquinone	1,4-NQ	1.20	33.7	11.7	28.2
1-Naphthaldehyde	1-NALD	0.67	3.42	1.81	5.1
2-Biphenylcarboxaldehyde	2-BPCA	0.11	7.64	1.98	71.4
9-Fluorenone	9-FLU	4.69	20.0	10.4	4.3
1,2-Acenaphthenequinone	1,2-ACEQ	7.35	64.0	17.8	8.7
9,10-Anthraquinone	9,10-AQ	9.71	43.1	15.8	4.4
1,8-Naphtalic anhydride	1,8-NA	1.06	38.5	7.69	36.4
2-Meth-9,10-anthraquinone	2-MAQ	4.82	24.2	12.4	5.0
Benzo[a]florenone	BAFLU	2.29	37.1	8.89	16.2
7H-Benzo[d,e]anthracen-7-one	BdeAQ	0.93	10.74	3.43	11.6
Benzo[a]anthracene-7,12-dione	BaAQ	0.41	8.24	2.22	20.0
5,12-Naphthacenequinone	5,12-NQ	0.01	1.86	0.77	329
6H-Benzo[c,d]pyren-6-one	BcdPQ	0.13	14.7	3.00	112
Polycyclic aromatic hydrocarbons	PAHs				
1,2,3,4-Tetrahydronapthalene	TH-NAPH	0.91	10.3	2.04	11.3
Naphthalene	NAPH	10.1	72.7	17.9	7.2
2-Methylnaphthalene	2-MNAPH	3.36	19.3	7.58	5.7
1-Methylnaphthalene	1-MNAPH	5.22	31.7	14.0	6.1
Biphenyl	BIPH	7.37	33.2	11.5	4.5
1,3-Dimethylnaphthalene	1,3-DMNAPH	9.25	68.5	22.4	7.4
Acenaphthylene	ACEY	0.32	2.29	0.65	7.1
Acenaphthene	ACEN	0.33	6.02	1.57	18.3
Fluorene	FLUO	2.18	17.5	3.78	8.0
Phenanthrene	PHE	14.8	81.6	23.9	5.5
Anthracene	ANT	1.82	14.9	3.48	8.2
2-Methylphenanthrene	2-MPHE	2.24	40.7	10.8	18.2
3,6-Dimethylphenanthrene	3,6-DMPHE	0.57	5.88	1.28	10.2
Fluoranthene	FLUA	0.71	13.0	2.52	18.3
Pyrene	PYR	2.09	25.9	4.95	12.4
Retene	RET	2.07	60.7	9.34	29.3
Benzo[a]anthracene	BaA	0.72	9.78	1.94	13.6
Chrysene+Triphenylene	CHR	1.61	20.7	3.77	12.8

Benzo[b+j+k]fluoranthene	BbjkF	3.76	47.7	10.2	12.7
Benzo[e]pyrene	BeP	2.55	15.1	4.56	5.9
Benzo[a]pyrene	BaP	0.49	14.6	1.80	30.1
Perylene	PER	5.55	39.5	14.5	7.1
Indeno [1,2,3-cd]pyrene	IcdP	0.73	13.7	2.50	18.7
Dibenzo[a,h]anthracene	DahA	0.47	4.84	1.35	10.4
Benzo[g,h,i]perylene	BghiP	1.58	26.0	4.79	16.5
Coronene	COR	1.17	8.53	2.62	7.3
Sum of azaarenes	∑4AZAs	4.97	23.0	11.6	4.6
Sum of oxygen-containing PAHs	∑15OPAHs	41.4	201.5	98.0	4.9
Sum of parent polycyclic aromatic hydrocarbons	∑29PAHs	109.3	628.4	188.0	5.7
∑PAHs without perylene	∑28PAHs	99.6	622.3	174.4	6.2
∑15OPAHs/∑28PAHs		0.31	1.21	0.65	3.9
Low molecular weight parent PAHs	LMW-PAHs	34.3	166.4	51.3	4.9
High molecular weight parent PAHs without perylene	HMW-PAHs	20.4	185.5	40.8	9.1
LMW-/HMW-PAHs		0.76	2.17	1.50	2.8
∑COM-PAHs [1]		17.2	172.3	36.8	10.0
∑COM-PAHs/∑28PAHs		0.13	0.31	0.19	2.4
Total nitrogen	TN	1.64	2.84	1.93	1.7
Total carbon	TC	49.7	62.7	55.5	1.3
Inorganic carbon	IC	11.5	38.4	27.8	3.3
Total organic carbon	TOC	17.2	43.2	27.7	2.5
Total sulfur	TS	2.28	4.47	3.53	2.0
TOC/TN	C/N	9.12	23.4	14.4	2.6
Loss on Ignition	LOI	0.10	0.20	0.14	2.0

[1] ∑COM-PAHs: Combustion derived PAH = sum of FLUA, PYR, BaA, CHR, BbjkF, BeP, BaP, IcdP and BghiP.

Table S2. Pearson correlation coefficients between sediment properties used in this study. **Bold** indicates that correlation is significant at the 0.01 level, and Underline indicates that correlation is significant at the 0.05 level in a two-tailed test.

	EC	Char	Soot	Char/ Soot	Σ OPAH	∑AZAs	Retene	Perylene	ΣPAHs	OPAH/ PAH	Σ LMW	Σ HMW	LMW/ HMW	ΣCOM	ΣCOM/ ΣPAHs	TOC	C/N
EC	1	**0.809**	0.161	**0.645**	0.269	0.031	0.149	0.043	0.145	0.117	0.152	0.19	-0.235	0.194	0.305	0.039	-0.089
Char	**0.809**	1	**-0.45**	**0.962**	-0.068	-0.251	-0.338	0.189	-0.371	0.356	-0.35	-0.316	0.115	-0.313	-0.051	-0.271	-0.122
Soot	0.161	**-0.45**	1	**-0.635**	**0.534**	**0.483**	**0.794**	-0.235	**0.844**	-0.433	**0.818**	**0.819**	**-0.550**	**0.820**	**0.548**	**0.515**	0.068
Char/Soot	**0.645**	**0.962**	**-0.635**	1	-0.137	-0.307	-0.419	0.202	**-0.491**	0.42	**-0.464**	**-0.445**	0.243	**-0.442**	-0.184	-0.341	-0.119
ΣOPAH	0.269	-0.068	**0.534**	-0.137	1	**0.676**	**0.69**	**-0.56**	**0.592**	0.376	**0.59**	**0.59**	-0.323	**0.593**	0.305	**0.559**	0.306
∑AZAs	0.031	-0.251	**0.483**	-0.307	**0.676**	1	**0.503**	**-0.608**	**0.529**	0.04	**0.48**	**0.515**	-0.452	**0.516**	0.293	**0.762**	**0.565**
Retene	0.149	-0.338	**0.794**	-0.419	**0.690**	**0.503**	1	-0.281	**0.905**	-0.233	**0.88**	**0.885**	**-0.513**	**0.888**	**0.577**	**0.547**	0.074
Perylene	0.043	0.189	-0.235	0.202	**-0.560**	**-0.608**	-0.281	1	-0.157	-0.388	-0.165	-0.186	0.073	-0.192	-0.044	**-0.515**	**-0.499**
ΣPAHs	0.145	-0.371	**0.844**	**-0.491**	**0.592**	**0.529**	**0.905**	-0.157	1	**-0.485**	**0.982**	**0.984**	**-0.647**	**0.984**	**0.692**	**0.609**	0.064
OPAH/PAH	0.117	0.356	-0.433	0.42	0.376	0.04	-0.233	-0.388	**-0.485**	1	-0.445	-0.448	0.347	-0.444	-0.32	-0.187	0.105
Σ LMW-PAH	0.152	-0.35	**0.818**	**-0.464**	**0.590**	**0.48**	**0.88**	-0.165	**0.982**	-0.445	1	**0.979**	**-0.582**	**0.978**	**0.698**	**0.577**	0.016
Σ HMW-PAH	0.19	-0.316	**0.819**	**-0.445**	**0.590**	**0.515**	**0.885**	-0.186	**0.984**	-0.448	**0.979**	1	**-0.714**	**1.00**	**0.793**	**0.581**	0.026
LMW/HMW	-0.235	0.115	**-0.55**	0.243	-0.323	**-0.452**	**-0.513**	0.073	**-0.647**	0.347	**-0.582**	**-0.714**	1	-0.711	**-0.87**	-0.409	-0.075
ΣCOM	0.194	-0.313	**0.82**	**-0.442**	**0.593**	**0.516**	**0.888**	-0.192	**0.984**	-0.444	**0.978**	**1.00**	**-0.711**	1	**0.795**	**0.582**	0.027
ΣCOM/ ΣPAHs	0.305	-0.051	**0.548**	-0.184	0.305	0.293	**0.577**	-0.044	**0.692**	-0.32	**0.698**	**0.793**	**-0.87**	**0.795**	1	0.29	-0.165
TOC	0.039	-0.271	**0.515**	-0.341	**0.559**	**0.762**	**0.547**	**-0.515**	**0.609**	-0.187	**0.577**	**0.581**	-0.409	**0.582**	0.29	1	**0.78**
C/N	-0.089	-0.122	0.068	-0.119	0.306	**0.565**	0.074	**-0.499**	0.064	0.105	0.016	0.026	-0.075	0.027	-0.165	**0.78**	1